Delft University of Technology

Aerodynamic and aeroacoustic effects of pylon trailing edge blowing on pusher propeller installation

Sinnige, T; Lynch, KP; Ragni, D; Eitelberg, G; Veldhuis, LLM

Aerodynamic and Aeroacoustic Effects of Pylon Trailing Edge Blowing on Pusher Propeller Installation

Tomas Sinnige[*], Kyle P. Lynch[†], Daniele Ragni[‡], Georg Eitelberg[§], and Leo L. M. Veldhuis[¶]

Delft University of Technology, Delft, 2629 HS, the Netherlands

The aerodynamic and aeroacoustic effects of pylon trailing edge blowing on the propulsive performance and noise emissions of a propeller installed in a pusher configuration were studied in a wind tunnel. A propeller model and a pylon equipped with a trailing edge blowing system were installed in the large low-speed facility of the German-Dutch wind-tunnels (DNW-LLF). Particle image velocimetry measurements of the flow field downstream of the pylon confirmed a wake re-energization obtained through blowing, with a momentum deficit recovery of 80% compared to the unblown case. For the symmetric inflow conditions considered, the effect of pylon installation on the propulsive performance was found small. Increases in thrust and torque of 1% up to 6% were measured at high and low thrust settings, which was comparable to the measurement variability. Acoustic data obtained using out-of-flow microphones confirmed the strong interaction effects resulting from the installation of the upstream pylon, with an increase in noise levels due to the presence of the pylon of up to 12 dB at a medium propeller thrust setting. The application of pylon trailing edge blowing successfully eliminated the installation effects, resulting in noise levels equal to those of the isolated propeller over the entire axial directivity range. At higher thrust settings the change in blade angle of attack due to the pylon wake impingement is smaller, and the steady blade loads are larger compared to the unsteady loads experienced during the wake passage. Consequently, in this operating regime the propeller noise emissions were dominated by steady sources for all but the most upstream observer positions.

I.   Introduction

The potential for an increase in propulsive efficiency makes the advanced propeller an interesting alternative to turbofans. Large rotor diameters combined with stringent interior noise constraints drive possible propeller aircraft design solutions to configurations with rear-fuselage mounted pusher propellers. In such a lay-out, the propeller blades rotate through the wake of the upstream pylon. The reduced inflow velocity experienced by the blades during the pylon wake passage leads to fluctuations in the blade sections' inflow angles. This results in unsteady blade loading and associated increased propeller noise emissions.

Pylon blowing can mitigate these adverse pylon interaction effects by eliminating the momentum deficit in the pylon wake. This has been shown previously by experimental research with single-rotating[1,2] and contra-rotating propellers,[3–6] as well as numerical investigations.[7] Although these studies all confirmed the potential of blowing as a means to reduce the pylon installation effects, no thorough quantitative data of the aerodynamic and aeroacoustic effects are yet available.

The experimental investigation discussed in the present manuscript aims at quantifying the aerodynamic and aeroacoustic installation effects resulting from the pylon - pusher propeller interaction, with and without pylon trailing edge blowing. An installed pusher configuration was simulated using a single-rotating tractor propeller model in combination with an upstream mounted pylon equipped with a trailing edge blowing system. The pylon installation effects occurring in this configuration have been found relevant for both single- and contra-rotating propeller configurations, since in the latter case the interaction effects resulting from the pylon wake impingement mainly affect the noise levels associated with the front rotor.[3–5,8,9]

---

[*]Ph.D. Student, Flight Performance and Propulsion Section, Faculty of Aerospace Engineering, AIAA member.
[†]Ph.D. Student, Aerodynamics Section, Faculty of Aerospace Engineering, AIAA member.
[‡]Assistant Professor, Wind Energy Section, Faculty of Aerospace Engineering, AIAA member.
[§]Full Professor, Flight Performance and Propulsion Section, Faculty of Aerospace Engineering, AIAA member.
[¶]Full Professor, Head of Flight Performance and Propulsion Section, Faculty of Aerospace Engineering, AIAA Member.

American Institute of Aeronautics and Astronautics

The study was part of the APIAN-INF experiment which was performed in the EU-funded ESWIRP project, and involved contributions from Airbus, Delft University of Technology, DLR, DNW, INCAS, TsAGI, TU Braunschweig, and the University of Cambridge.

II.   Experimental Setup and Methodology

A.   Wind Tunnel Facility and Models

The experiments were performed in the large low-speed facility (LLF) of the German-Dutch wind tunnels (DNW). An open jet configuration with 8 m x 6 m outlet was selected, resulting in a wind speed range of $0 - 80$ m/s. At the position of the model in the tunnel the turbulence level is smaller than 0.02%, and the total pressure deviations are less than 0.1%. The test hall, measuring approximately 50 m x 30 m x 20 m, is treated with acoustic lining to result in a semi-anechoic environment. The wind tunnel is known to have a low background noise level, which was further improved by recent upgrades of the turning vane geometry and the heat exchanger – flow straightener assembly.[10] An overview of the test setup is shown in Fig. 1.
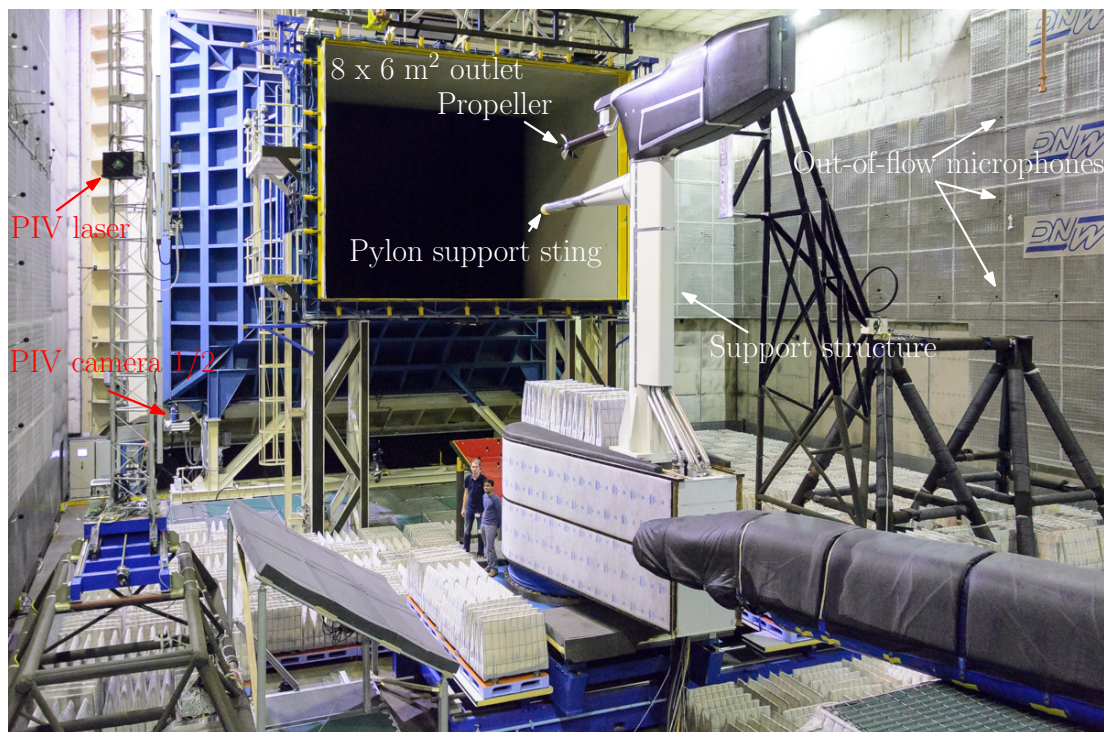

Figure 1. Overview of the experimental setup.

The propeller model (Fig. 2) was originally built for the European APIAN (Advanced Propulsion Integration Aerodynamics and Noise)[11–14] project. It features six carbon fiber blades and a rotor diameter of 0.508 m. The blade angle at 75% of the radius was set to 40.4 degrees. A six-component Rotating Shaft Balance (RSB) is integrated in the propeller model as discussed in more detail in Subsection B.

The pylon model (Fig. 3) was positioned at a fixed spacing of approximately 30% of the propeller diameter upstream of the propeller. The design of the pylon features a straight, untapered planform with a chord length of 0.489 m. The cross-section is defined by a NACA0010 profile, modified to have a trailing edge thickness of 0.8% of the chord. A fixed support sting was used to mount the pylon to the structure holding the propeller. For comparison reasons this sting was not removed during measurements without the pylon. A pylon blowing system was installed in the aft part of the model, with its outlet integrated in the trailing edge. The blowing system was designed with the goal to obtain a uniform outflow velocity along its span, adopting the Uniform Blowing Rod (UBR) concept previously discussed in Ref. 2. The UBR is operated in non-choked conditions, hence the uniformity of the outflow velocity profile is governed by the design of the blowing channel. The final design featured a blowing slit with a thickness of 2 mm and a span of 276 mm. In this way, the blowing system covered the propeller blades over the radial range of $0.11 \leq r/R \leq 1.15$. A cross-sectional drawing of the interior of the resulting blowing system is presented in Fig. 4.
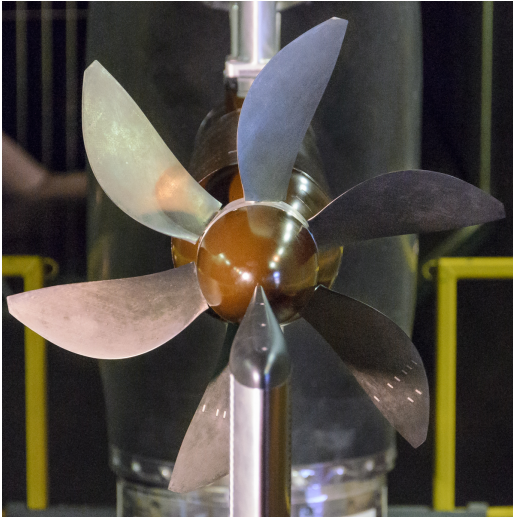
American Institute of Aeronautics and Astronautics

Figure 2. APIAN propeller model positioned downstream of the pylon model.

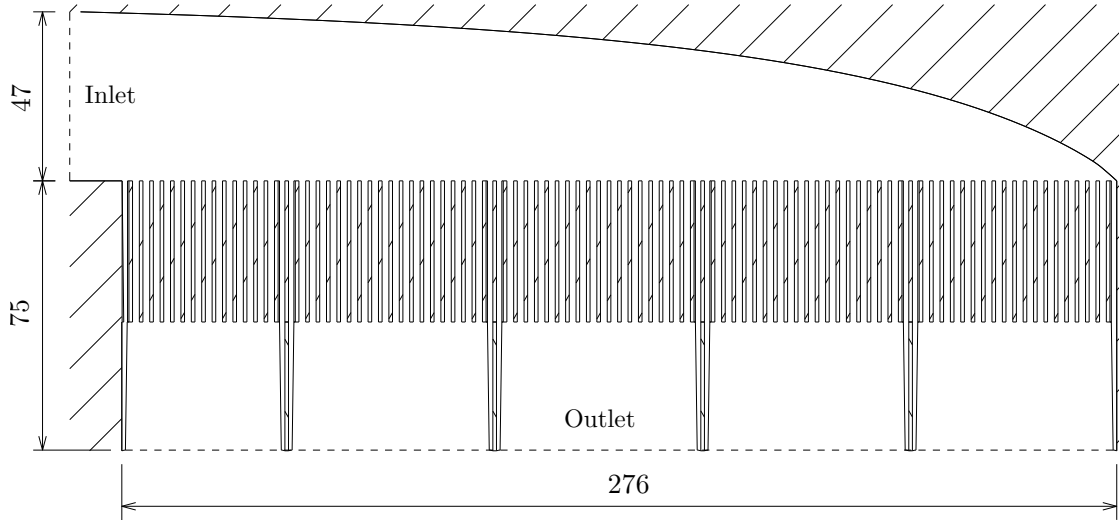**Figure 3. Pylon model installed upstream of the APIAN propeller model.**

Figure 4. Cross-sectional drawing of the interior of the pylon blowing system; dimensions in millimeters.

The flow rate delivered through the pylon blowing system to the wind tunnel flow was actively monitored and controlled by a mass flow controller installed at the bottom of the support structure. Measurements were taken at different blowing rates to assess the sensitivity of the pylon installation effects to the degree of pylon wake filling. A pylon blowing mass flow coefficient $c_{\dot{m}}$ was defined as follows:

$$c_{\dot{m}} = \frac{\dot{m}}{\rho_\infty U_\infty A_{\text{slit}}} \tag{1}$$

with $\dot{m}$ the measured pylon blowing mass flow, ρ_∞ the freestream density, U_∞ the freestream velocity, and A_{slit} the outflow area of the blowing slit.

B. Experimental Techniques

Several measurement techniques were used to quantify the aerodynamic and aeroacoustic change in performance and flow behavior due to the pylon – propeller interaction effects with and without blowing. Measurements of the propulsive performance were carried out via a three-spoke, six-component RSB integrated in the propeller model. The two out-of-plane components (thrust and torque) were directly measured by the RSB, while the remaining forces and moments followed from a decomposition of the two in-plane components. For a detailed description of the working principles of rotating shaft balances the reader is referred to Refs. 15 and 16.

Stereoscopic PIV was employed to obtain quantitative information of the velocity deficit in the flow field behind the pylon trailing edge. Phase-locked measurements were performed at eleven different angular blade positions, separated by six degrees. Per phase angle thirty images were acquired to allow for averaging of the instantaneous flow fields into a converged mean. All results discussed in the present manuscript are based on an average over all phase angles considered. An automated traversing system was used to simultaneously move lasers and cameras in the vertical direction. Table 1 presents an overview of the most important parameters of the PIV setup and data acquisition characteristics.

Table 1. PIV setup and data acquisition characteristics.

Parameter	Value	Parameter	Value
Laser	Quantel Evergreen Nd:YAG 200 mJ	Magnification	0.040
Cameras	2x PCO SensiCam	Digital resolution	6.0 px/mm
Image sensor size	1,280 px x 1,024 px	Pulse separation	$15 - 20\ \mu s$
Pixel size	6.7 μm x 6.7 μm	Freestream shift	$5 - 7$ px
Objective	Zeiss 200mm f/2.0 + 2x teleconverter	Phase angle separation	6 deg
Effective focal length	400 mm	Samples per phase angle	30
Effective aperture	f/4.0		

To quantify the aeroacoustic impact of the pylon installation effects, 48 out-of-flow microphones installed on the wall of the test hall were used. Half of the available microphones were positioned at approximately the same vertical position as the propeller, corresponding to a circumferential directivity angle of $\phi_0 = 0°$. These microphones covered a geometric axial directivity range of $35° \leq \theta \leq 145°$, not taking into account shear layer refraction effects. The definition of the axial and circumferential directivity angles θ and ϕ used in this manuscript is given in Fig. 5. The microphones positioned at vertical positions above and below the propeller ($\phi_0 \pm 10°$) covered a similar axial directivity range, but at half the angular resolution.
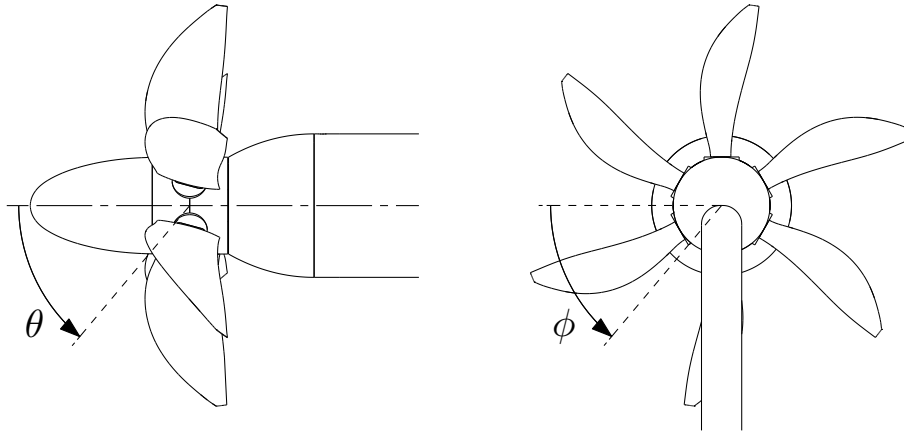

Figure 5. Definition of axial and circumferential directivity angles θ and ϕ.

C. Analyzed Test Cases

The measurements were performed at the operating conditions given in Table 2.

Table 2. Overview of the analyzed test cases.

Parameter	Symbol	Value
Freestream velocity	U_∞	60 m/s
Advance ratio	J	1.05, 1.40, 1.75
Angle of attack	α	0°
Angle of sideslip	β	0°
Pylon blowing mass flow coefficient	$c_{\dot{m}}$	0.0, 1.4, 1.6, 1.8
Radial stations PIV planes	$(r/R)_{\mathrm{PIV}}$	0.34, 0.49, 0.69, 0.79, 0.89, 0.99

American Institute of Aeronautics and Astronautics

Three propeller advance ratios ($J = 1.05, 1.40, 1.75$) were considered for the PIV and acoustic measurements, corresponding to a relatively "high", "medium", and "low" thrust setting. The propeller propulsive performance was evaluated at additional advance ratios. All measurements discussed in this paper were performed in symmetric inflow conditions ($\alpha = \beta = 0°$). Before the start of the final test program the propeller noise emissions were evaluated at a single operating point for a full range of blowing rates. The blowing coefficient resulting in the largest noise reductions was selected for the subsequent measurements with blowing enabled, together with blowing coefficients equal to 85% and 115% of the optimum.

III.   Results

A.   Pylon Blowing System Outflow

To characterize the outflow from the pylon blowing system, the velocity downstream of the blown pylon was measured in a separate test setup at zero freestream velocity. The blown mass flow was set to a value corresponding to the design blowing coefficient of 1.4 at a freestream velocity of 60 m/s. A total pressure probe was traversed in the vertical direction along the span of the pylon, centered with respect to the blowing slit. Figure 6 displays the resulting outflow velocity versus the pylon spanwise coordinate y/b, measured from the root of the model. Although these measurements were performed without the propeller present, the corresponding radial coordinates of the downstream blade in the final test setup are also indicated. The data were obtained at ten percent of the propeller diameter behind the trailing edge of the blowing system. The four support struts in the blowing slit (see Fig. 4) are identified in Fig. 6 by the red dashed lines.
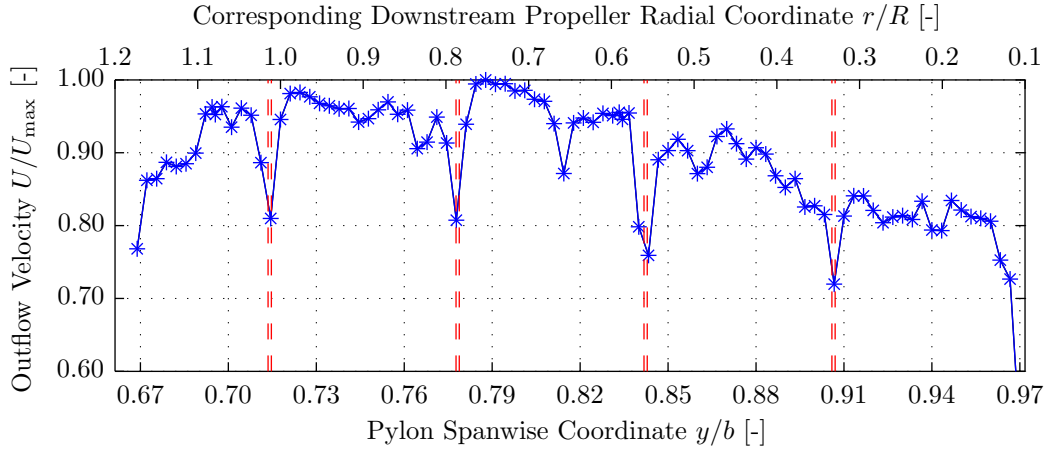

Figure 6. Pylon blowing system outflow velocity profile; $\Delta X/D_{\mathrm{prop}} = 0.1$, $U_\infty = 0$ m/s, $c_{\dot{m}}^{U_\infty=60\mathrm{m/s}} = 1.4$.

Figure 6 shows that the outflow from the pylon blowing system is reasonably uniform for $0.70 < y/b < 0.83$, with outflow velocities within 5% of the maximum exit velocity. This part of the blowing system is positioned upstream of the outboard part of the blade ($0.6 \leq r/R \leq 1.0$). Towards the tip of the pylon, corresponding to the inboard propeller radial stations ($r/R < 0.6$), the outflow velocity decreases down to 80% of the maximum velocity at the most inboard radial station covered by the blowing slit. The four dips in outflow velocity at the spanwise coordinates of 0.71, 0.78, 0.84, and 0.91 correspond to the wakes of the four support struts in the blowing slit.

B.   Pylon Wake Velocity Profiles

With the pylon installed upstream of the propeller, the blades experience a periodic change in inflow velocity due to the presence of the pylon wake. The magnitude of the resulting angle of attack perturbation is governed by the amplitude of the velocity deficit in the pylon wake. Hence, the unsteady blade forces and resulting noise emissions are a function of the characteristics of the pylon wake directly upstream of the propeller. Knowledge of the local velocity profiles is therefore important to understand the pylon installation effects. To measure the pylon wake velocity profiles, PIV planes were positioned between the pylon trailing edge and the propeller. As such, the effect of the downstream propeller on the pylon wakes was inherently taken into account. Figure 7 displays two examples of velocity fields obtained from the PIV measurements. On the left the unblown case is considered, while the flow field on the right was obtained at a blowing coefficient of $c_{\dot{m}} = 1.62$. In addition to the mean velocity fields depicted in Fig. 7, Fig. 8 presents the corresponding root mean square deviations of the instantaneous velocities relative to the local average.
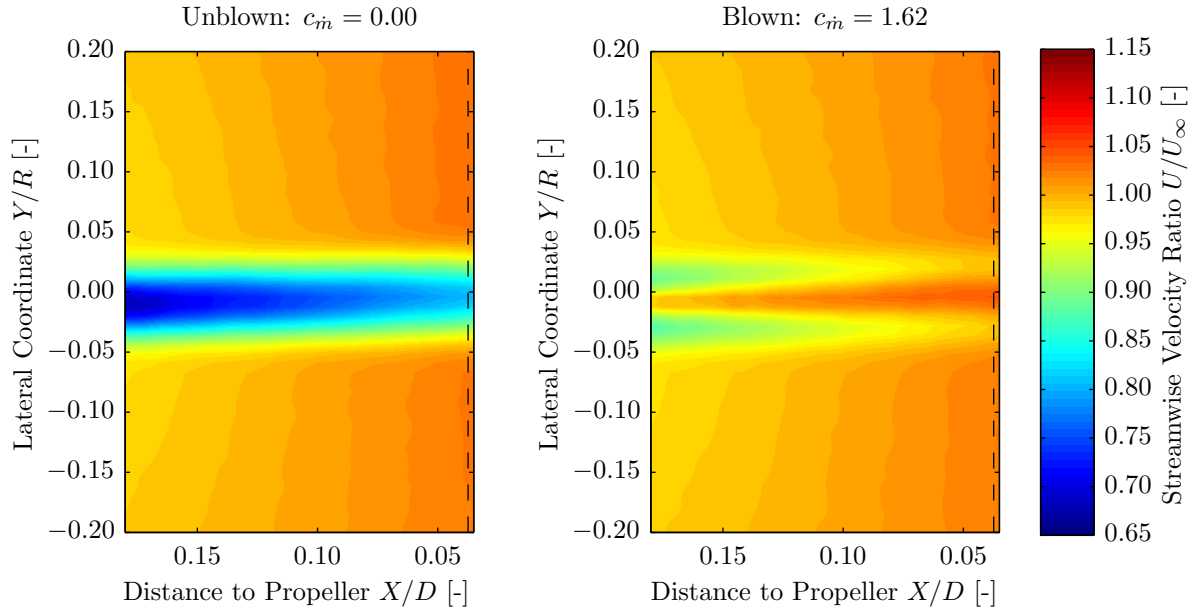
Figure 7. Non-dimensional average streamwise velocity component behind the pylon trailing edge with and without pylon blowing; $r/R = 0.79$, $J = 1.40$.
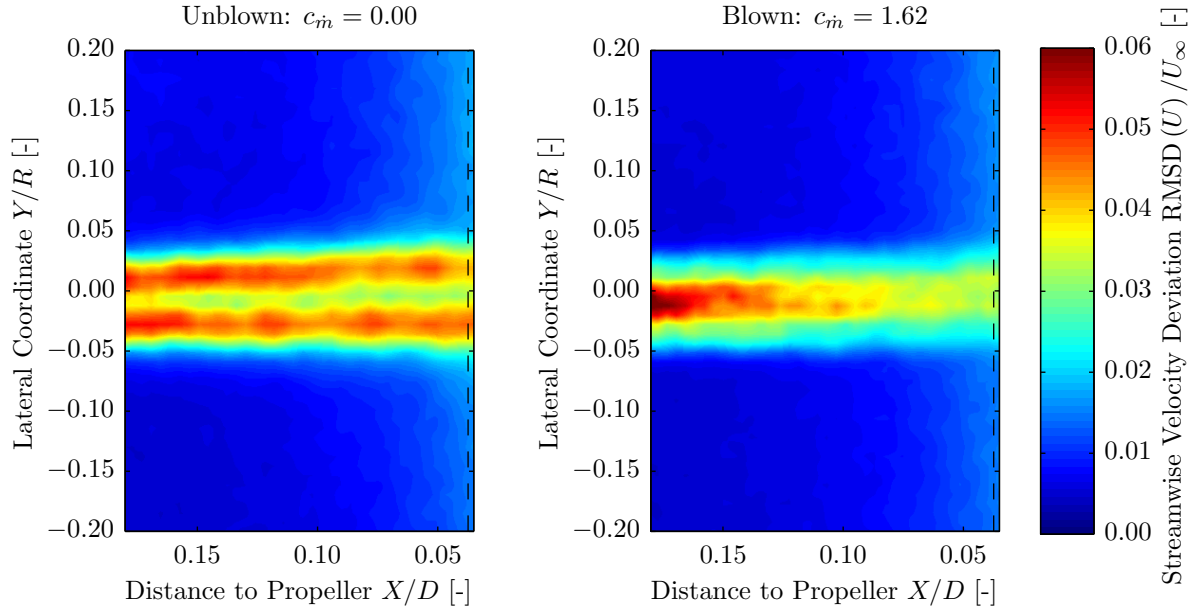

Figure 8. Non-dimensional root mean square deviation of the instantaneous streamwise velocity component behind the pylon trailing edge with and without pylon blowing; $r/R = 0.79$, $J = 1.40$.

Figure 7 shows the presence of the momentum deficit in the pylon wake, which is refilled by the additional mass flow and re-energizing effect introduced by blowing. In the unblown case the maximum velocity deficit directly upstream of the propeller amounts to 20% of the freestream velocity. In the blown configuration at this streamwise position the velocity in the wake center is approximately recovered to the undisturbed value. For both cases the velocity gradient outside of the pylon wake is due to the suction by the propeller.

The deviations of the instantaneous streamwise velocity component in the wake regions depicted in Fig. 8 are the result of modulation of the pylon wake, and lead to additional broadband noise emissions compared to the configuration without pylon. It is observed that application of blowing reduces the magnitude of the instantaneous velocity fluctuations in the pylon wake. Whereas in the unblown case the root mean square deviation of the velocity directly upstream of the propeller equals three to five percent of the freestream velocity, with blowing enabled this is decreased to two to four percent. The fluctuations outside of the pylon wake are non-zero due to the changes in the flow field imposed by the propeller at the different phase angles.

To quantitatively assess the effects of the employment of the blowing system on the pylon wake velocity deficit, velocity profiles were extracted along the dashed lines indicated in Figs. 7 and 8. The resulting data are shown in Fig. 9, which also contains the velocity profiles measured at two additional blowing coefficients.
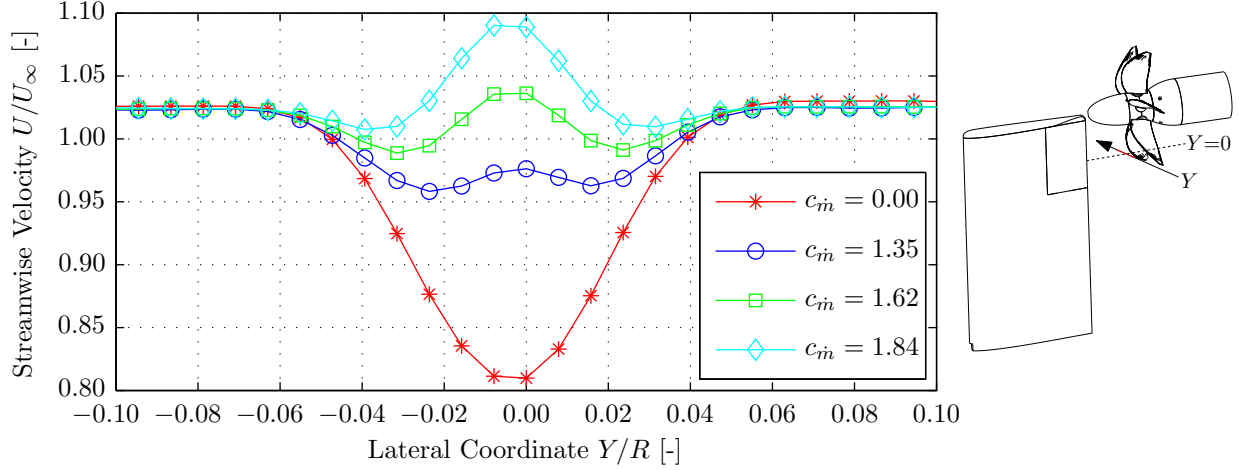

Figure 9. Pylon wake velocity profiles; $\Delta X/D = 0.04$, $r/R = 0.79$, $J = 1.40$.

Figure 9 confirms the reduction in velocity deficit in the pylon wake due to blowing. Because of the small thickness of the blowing slit in the trailing edge of the model the resulting wake profiles did not become completely uniform, but instead displayed a velocity overshoot on the wake centerline. To quantify the sensitivity of the wake profiles to the blowing coefficient, a non-dimensional integral velocity deficit parameter ξ is introduced as follows:

$$\xi = \int\limits_{-b_{\mathrm{w}}/R}^{+b_{\mathrm{w}}/R} \left| 1 - \frac{U}{U_{\mathrm{e}}} \right| \mathrm{d}\frac{Y}{R} \tag{2}$$

with b_{w} the wake half-width, U the local streamwise velocity component, U_{e} the streamwise velocity at the wake edge, and Y/R the lateral coordinate nondimensionalized with the propeller radius.

For the wake profiles given in Fig. 9, at the optimal blowing coefficient of $c_{\dot{m}} = 1.62$ the integral wake velocity deficit is decreased by 80% compared to the unblown case. As shown in Fig. 6, the outflow velocity from the blowing system was not completely constant in the spanwise direction. To assess the effect of the variations in outflow velocity on the blown pylon wake profiles, the wake flow fields were measured downstream of a range of spanwise positions. Figure 10 presents the values of the integral velocity deficit parameter ξ versus the coordinate of the downstream propeller radial station for the unblown and blown cases. For reference the corresponding pylon spanwise coordinates are also indicated. For the measurement plane closest to the tip of the pylon (corresponding to $r/R = 0.34$) the most extreme part of the wake ($0.05 \le Y/R \le 0.10$) was obscured from the cameras due to the presence of the spinner. For these cases the profiles were completed by assuming symmetry around the wake center.

From Fig. 10 it is observed that the employment of blowing clearly reduces the integrated velocity deficit in the pylon wake. In the unblown configuration the integrated velocity deficit is approximately constant at the spanwise positions upstream of the outboard part of the blade ($r/R \ge 0.69$). At the more inboard radial stations the integral velocity deficit is larger due to three-dimensional tip effects and interactions with the spinner. Upstream of the most inboard radial station considered ($r/R = 0.34$) the interactions with the spinner result in a natural wake filling, leading to a smaller integral velocity deficit than at $r/R = 0.49$.

With pylon blowing enabled, the best wake filling is achieved at a blowing coefficient of $c_{\dot{m}} = 1.62$ at all radial positions except the most inboard. The average decrease in integral wake velocity deficit at this optimal blowing coefficient is around 80% compared to the unblown configuration, except upstream of the most inboard radial station at which a smaller reduction of 60% is achieved. The latter is expected considering the lower outflow velocities obtained from the blowing system in this region as shown previously in Fig. 6. This also explains the better wake filling at the highest blowing coefficient upstream of the most inboard radial station considered.
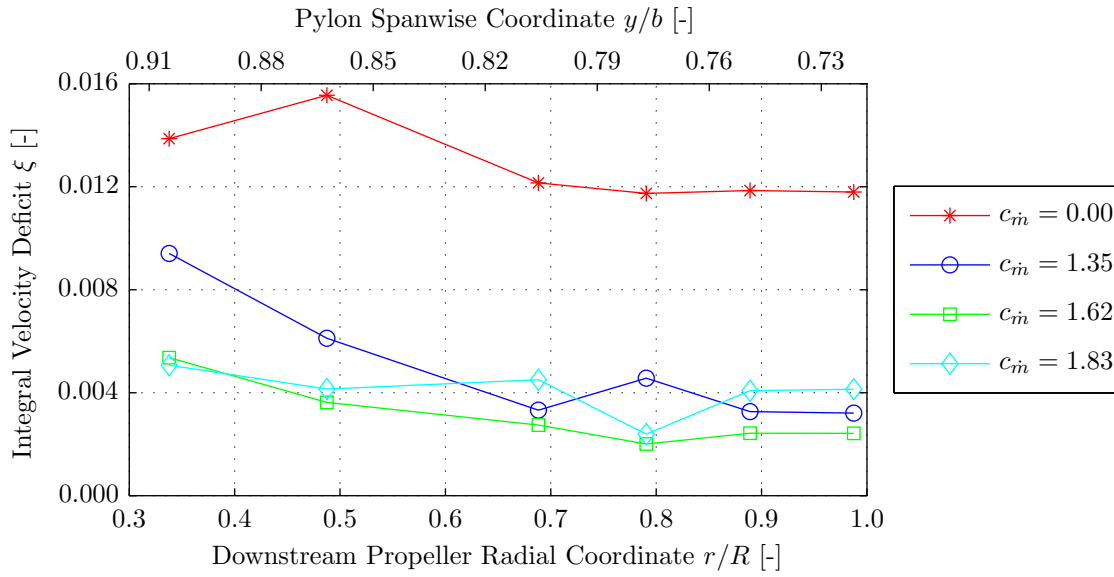
American Institute of Aeronautics and Astronautics

Figure 10. Non-dimensional integral wake velocity deficit versus downstream propeller radial coordinate for different blowing coefficients; $\Delta X/D = 0.04$, $J = 1.40$.

C. Propeller Propulsive Performance

The propeller propulsive performance was evaluated during all measurements using the RSB. The resulting data were expressed in terms of the thrust coefficient C_T, torque coefficient C_Q, and propeller efficiency η:

$$C_T = \frac{T}{\rho_\infty n^2 D^4} \qquad (3) \qquad\qquad C_Q = \frac{Q}{\rho_\infty n^2 D^5} \qquad (4) \qquad\qquad \eta = \frac{J}{2\pi}\frac{C_T}{C_Q} \qquad (5)$$

with D the propeller diameter, J the advance ratio ($J = \frac{U_\infty}{nD}$), n the rotational speed of the propeller in revolutions per second, Q the torque, T the thrust, and ρ_∞ the freestream density.

The measured integral propeller performance diagrams for the isolated and installed configurations are given in Fig. 11. Estimations of the variations of repeated measurements were computed from the multiple data points at advance ratios of 1.05, 1.40, and 1.75 and are indicated by the error bars.
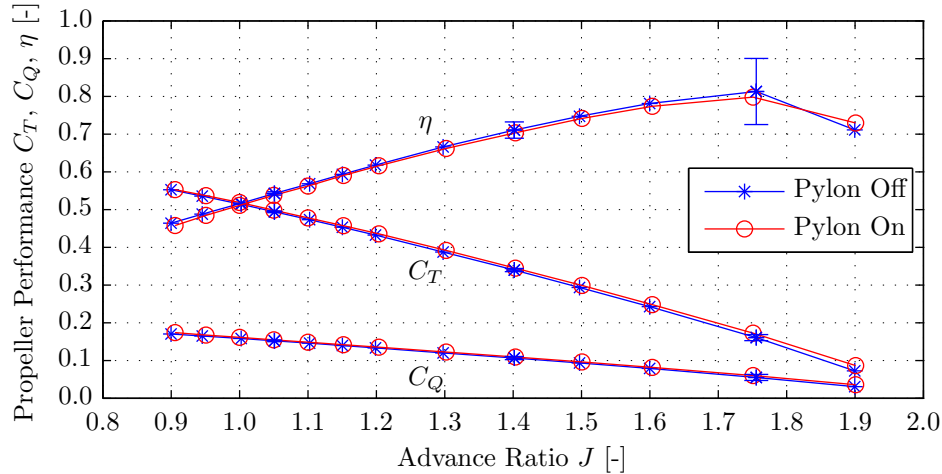

Figure 11. Effect of pylon installation on the propeller propulsive performance.

Figure 11 shows the expected quasi-linear behavior of thrust and torque coefficient versus advance ratio. At lower advance ratios the performance curves start to flatten due to flow separation on the blades. Compared to the isolated configuration, installation of the pylon increases the thrust and torque by 1% up to 6% at advance ratios of 1.05 and 1.75, respectively. These differences are however approximately within the variations of repeated measurements, which for the thrust coefficient amount to 1% at $J = 1.05$ up to 5% at $J = 1.75$. Nevertheless, the increase in thrust and torque is the expected result of the locally reduced

American Institute of Aeronautics and Astronautics

advance ratio in the pylon wake, and was also observed before in a numerical analysis of a contra-rotating open rotor.[9] Experiments with a single-rotating propeller also showed increased performance in the installed configuration.[1] However, this was attributed to the influence of the upstream nacelle (not present in the study discussed in the current manuscript) rather than the pylon.

D. Propeller Noise Emissions

Compared to the isolated propeller, with the pylon installed the unsteady blade loads resulting from the pylon wake impingement lead to an additional noise generating mechanism. This increases the amplitude of the propeller tones, while also the directivity is changed. By decreasing the velocity deficit in the pylon wake, employment of pylon blowing can mitigate these adverse installation effects. Figure 12 presents the sound spectra corresponding to the isolated, unblown, and blown configurations as measured in the propeller plane, perpendicular to the pylon. For the measurements with blowing enabled the blowing coefficient was set to the optimal value identified from the PIV measurements discussed in Subsection B. At the selected operating conditions the blade passage frequency (BPF) equals 509 Hz. The part of the spectrum below 250 Hz is omitted since here the measured sound pressure levels are dominated by wind tunnel fan and background noise. The results in Fig. 12 are presented as measured; the sound pressure levels are not scaled to a desired source-observer distance and shear layer refraction effects are not corrected for.
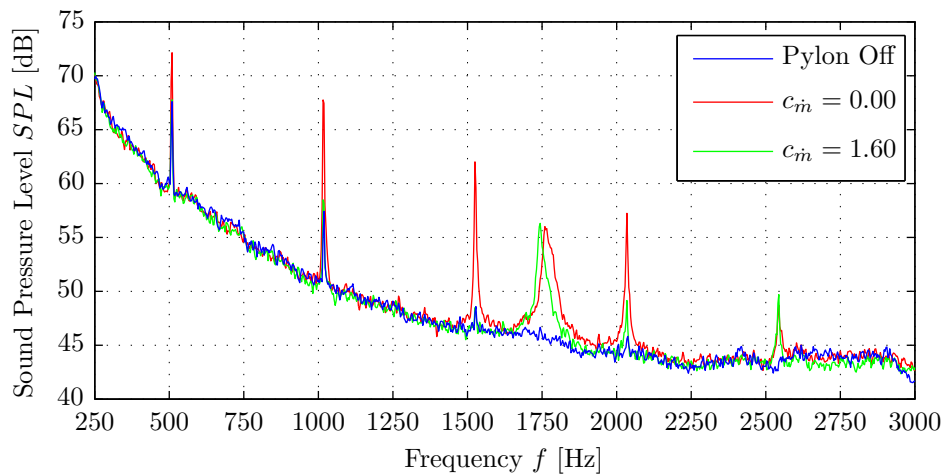

Figure 12. Sound spectra in isolated, unblown ($c_{\dot{m}} = 0.00$), and blown ($c_{\dot{m}} = 1.60$) configurations; $\theta = 90°$, $\phi = 0°$, $J = 1.40$.

Figure 12 substantiates the strong impact of the pylon on the noise emissions. Whereas for the isolated propeller only the first two tones stand out of the background noise levels, with the unblown pylon present the higher harmonics are also clearly recognizable. For the fundamental tone a noise increase of 5 dB is measured, while at twice the BPF the level is raised by 10 dB. These differences are significant compared to the measurement uncertainty of less than 1 dB, as identified from repeated measurements at constant operating conditions. The effect of the pylon on the broadband levels could not be assessed, since background noise from the tunnel fan and inflow infrastructure dominated the broadband components of the spectra.

Application of trailing edge blowing successfully mitigates the installation penalty, bringing the sound pressure levels of the first three propeller tones back to the values observed for the isolated configuration. For the higher harmonics some remaining noise increase is left in the blown configuration. This is attributed to the remaining non-uniformities in the blown pylon wakes as discussed in Subsection B. The tonal noise component observed around a frequency of 1,750 Hz for the two cases with pylon installed is the result of vortex shedding from the pylon trailing edge. This was confirmed by the PIV measurements of the lateral velocity fields directly behind the pylon trailing edge.

To analyze the noise penalty due to pylon installation in more detail, Fig. 13 presents the change in total tonal sound pressure level resulting from the installation of the pylon. The levels measured for the isolated propeller are used as baseline. The total tonal sound pressure levels are defined as the sum of the levels of the first six propeller tones, and are scaled to an observer distance of ten times the propeller diameter. The measurements are taken at a circumferential directivity angle perpendicular to the pylon ($\phi = 0°$). The unblown and blown configurations are considered, with the blown data obtained at the mass flow coefficient for optimal wake filling ($c_{\dot{m}} = 1.60$).
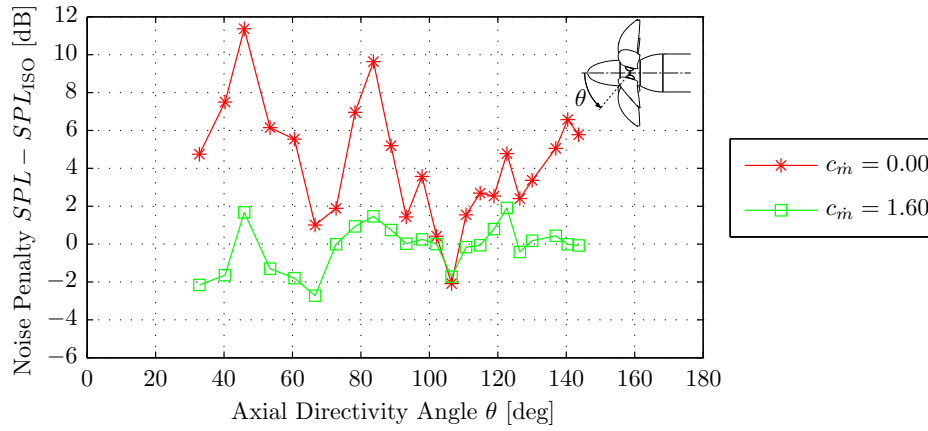
Figure 13. Change in total tonal sound pressure level due to installation of the pylon with and without blowing at a medium thrust setting, relative to the levels measured for the isolated configuration; $\phi = 0°$, $J = 1.40$.

Figure 13 confirms the observation made earlier that the installation of the unblown pylon strongly increases the tonal noise levels. Depending on the axial directivity angle, a noise increase of up to 12 dB is observed compared to the isolated propeller. The application of blowing successfully eliminates the installation effects, by bringing back the noise penalty to values around 0 dB at all axial directivity angles.

The unexpected peak in the noise penalty for the unblown configuration around an axial directivity angle of $\theta = 80°$ is the result of a local dip in the noise levels measured for the isolated propeller. Based on previous experience it was hypothesized that this was due to aerodynamic interference effects with the downstream support structure or other inflow infrastructure, possibly leading to an asymmetry in the inflow to the propeller. The resulting unsteady blade loads then introduce an additional noise generating mechanism, which interferes with the steady sources. With the unblown pylon installed this asymmetry is still present, however it is no longer observed in the total sound pressure level since that is now dominated by the noise emissions due to the pylon wake impingement. Consequently, around $\theta = 80°$ the measured difference between the noise emissions for the configurations with and without pylon is expected to be larger than if this asymmetric inflow would not have been present. Numerical simulations of the flow field around the entire wind tunnel setup are required to support this hypothesis.

Considering that the perturbation due to the pylon wake is in the inflow direction, it can be expected that the impact of the pylon installation will depend on the rotational speed of the propeller. At higher advance ratios the relative effect of the reduced inflow velocity is larger than at lower advance ratios, for which the high rotational speed decreases the amplitude of the angle of attack fluctuations experienced by the blades. More importantly, the higher steady blade loading at lower advance ratios will decrease the relative impact of the resulting unsteady loads. To confirm this hypothesis, noise measurements with and without pylon were also performed at a higher thrust setting, corresponding to an advance ratio of $J = 1.05$. Figure 14 shows the noise penalty due to installation at this advance ratio, again for the blown and unblown cases.
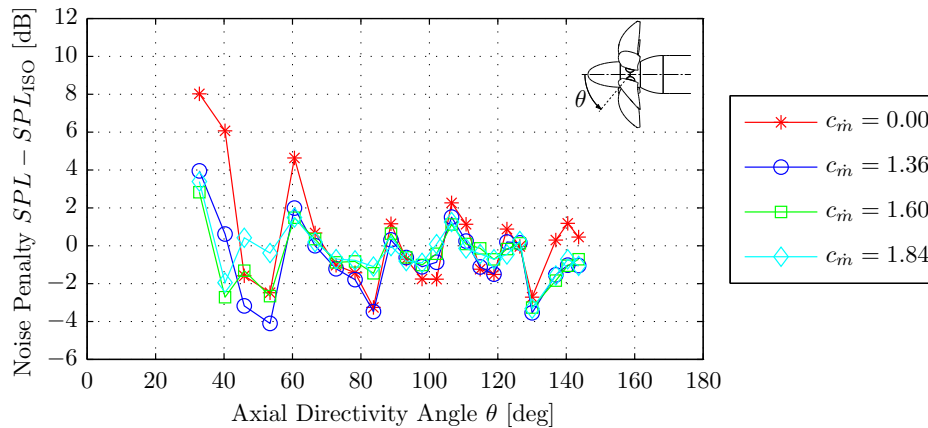

Figure 14. Change in total tonal sound pressure level due to installation of the pylon with and without blowing at a high thrust setting, relative to the levels measured for the isolated configuration; $\phi = 0°$, $J = 1.05$.

American Institute of Aeronautics and Astronautics

The data displayed in Fig. 14 confirm the expected result of smaller installation penalty at lower advance ratio. Instead of the clear increase in noise levels over the entire directivity range observed in Fig. 13 for $J = 1.40$, at $J = 1.05$ the noise penalty due to installation fluctuates around 0 dB for all but the most upstream angles. For $60° \leq \theta \leq 140°$ the steady sources due to blade thickness and steady-state loading dominate the propeller noise emissions, and the installation of the pylon does not affect the overall sound pressure level. In the most upstream domain the presence of the pylon does increase the noise emissions. Employment of blowing reduces the noise penalty at these angles, although not all of the noise increase in the upstream arc can be recovered.

IV.   Conclusions

The pylon – propeller interaction effects associated with pusher propellers were studied in a large-scale wind tunnel. From the results presented in this paper the following conclusions were drawn:

- A pylon trailing edge blowing system was designed with the goal to obtain uniform outflow, which was achieved over the region upstream of the outboard part of the propeller blade ($0.6 \leq r/R \leq 1.0$). Below this radial station range the outflow velocities decreased gradually, down to a minimum of 80% of the maximum outflow velocity at the tip of the blowing system.

- The pylon wake measurements using PIV showed that application of the pylon trailing edge blowing system indeed decreased the velocity deficit in the pylon wake. Because of the small thickness of the blowing slit the resulting wake profiles did not become completely uniform, but instead displayed a local maximum on the wake centerline. At the optimal blowing coefficient a reduction in integrated velocity deficit of up to 80% was achieved compared to the unblown configuration.

- From the propeller propulsive performance measurements it was concluded that, for the symmetric inflow conditions considered in this paper, the effect of pylon installation on the integral propeller performance is small. Increases in thrust and torque of 1% up to 6% were observed at high and low thrust settings, respectively, which however was comparable to measurement variability. Nevertheless, the increase in thrust and torque is the expected result of the locally reduced advance ratio in the pylon wake.

- Analyses of the out-of-flow microphone data confirmed the pronounced effects of installation of the upstream pylon on the propeller noise emissions, with an increase in tonal noise levels of up to 12 dB compared to the isolated case at a medium propeller thrust setting ($J = 1.40$). Application of the pylon trailing edge blowing system successfully mitigated the installation effect. At the optimal blowing coefficient identified from the wake measurements the sound pressure levels were reduced to the values recorded for the isolated propeller. At lower advance ratios the change in blade angle of attack due to the pylon wake impingement is smaller, and the steady blade loads are larger compared to the unsteady loads experienced during the wake passage. Consequently, at $J = 1.05$ it was found that installation of the pylon only affected the noise levels in the most upstream arc ($\theta \leq 60°$). In the rest of the domain the noise emissions were dominated by steady sources.

Acknowledgments

References

[1]Gentry, G. L., Jr., Booth, E. R., Jr., and Takallu, M. A., "Effect of Pylon Wake With and Without Pylon Blowing on Propeller Thrust," 1990, NASA-TM-4162.

[2]Sinnige, T. and Veldhuis, L. L. M., "Pylon Trailing Edge Blowing Effects on the Performance and Noise Production of a Pusher Propeller," *52nd Aerospace Sciences Meeting*, 2014, National Harbor, MD, USA.

[3]Shivashankara, B., Johnson, D., and Cuthbertson, R., "Installation Effects on Counter Rotating Propeller Noise," *13th AIAA Aeroacoustics Conference*, 1990, Tallahassee, FL, USA.

[4]Ricouard, J., Julliard, E., Omaïs, M., Regnier, V., Parry, A. B., and Baralon, S., "Installation effects on contra-rotating open rotor noise," *16th AIAA/CEAS Aeroacoustics Conference*, 2010, Stockholm, Sweden.

[5]Paquet, C., Julliard, E., Genoulaz, N., Ricouard, J., and Spiegel, P., "Z08: low-speed aero-acoustic experimental characterization of open rotor installation on aircraft," *20th AIAA/CEAS Aeroacoustics Conference*, 2014, Atlanta, GA, USA.

[6]Fernando, R. and Leroux, M., "Open-Rotor low speed aero-acoustics: wind tunnel characterization of an advanced blade design in isolated and installed configurations," *20th AIAA/CEAS Aeroacoustics Conference*, 2014, Atlanta, GA, USA.

[7]Stürmer, A. and Yin, J., "Pylon Trailing Edge Blowing for the Control of CROR Unsteady Blade Loads," *New Results in Numerical and Experimental Fluid Mechanics VIII*, edited by A. Dillmann, G. Heller, H.-P. Kreplin, W. Nitsche, and I. Peltzer, Vol. 121 of *Notes on Numerical Fluid Mechanics and Multidisciplinary Design*, Springer Berlin Heidelberg, 2013, pp. 715–722.

[8]Peake, N. and Parry, A. B., "Modern Challenges Facing Turbomachinery Aeroacoustics," *Annual Review of Fluid Mechanics*, Vol. 44, 2012, pp. 227–248.

[9]Stürmer, A. and Yin, J., "Aerodynamic and Aeroacoustic Installation Effects for Pusher-Configuration CROR Propulsion Systems," *28th AIAA Applied Aerodynamics Conference*, 2010, Chicago, IL, USA.

[10]Holthusen, H., Bergmann, A., and Sijtsma, P., "Investigations and measures to improve the acoustic characteristics of the German-Dutch Wind Tunnel DNW-LLF," *18th AIAA/CEAS Aeroacoustics Conference*, 2012, Colorado Springs, CO, USA.

[11]Polacsek, C., Spiegel, P., Boyle, F., Eaton, J., Brouwer, H., and Nijboer, R., "Noise Computation of High-Speed Propeller-Driven Aircraft," *6th AIAA/CEAS Aeroacoustics Conference*, 2000, Lahaina, HI, USA.

[12]Bousquet, J.-M. and Gardarein, P., "Recent improvements in Propeller Aerodynamic computations," *18th AIAA Applied Aerodynamics Conference*, 2000, Denver, CO, USA.

[13]Philipsen, I., Hoeijmakers, H., and Hegen, S., "An Overview of Advanced Propeller Simulation Tests in the German Dutch Wind Tunnels (DNW)," *22nd AIAA Aerodynamic Measurement Technology and Ground Testing Conference*, 2002, St. Louis, MO, USA.

[14]Crozier, P., "APIAN Installed Tests in the ONERA S1MA Wind Tunnel," *39th AIAA Aerospace Sciences Meeting & Exhibit*, 2001, Reno, NV, USA.

[15]Custers, L. G. M., Hoeijmakers, A. H. W., and Harris, A. E., "Rotating shaft balance for measurement of total propeller force and moment," *15th International Congres on Instrumentation in Aerospace Simulation Facilities*, 1993, Saint-Louis, France.

[16]Bret, J. F., Leconte, P., Vieira, J. P., Fetet, T., and Séchaud, J. F., "Rotating Shaft Balances for CRORs and Propellers," *53rd AIAA Aerospace Sciences Meeting*, 2015, Kissimmee, FL, USA.